**Mesoscale Patterns Supporting EF3-EF5
Tornadoes across Eastern Kansas and Vicinity**

William P. Gargan
National Weather Service, Topeka, Kansas

Ryan C. Bunker
National Weather Service, Topeka, Kansas
University of Oklahoma, Norman, Oklahoma

Bryan M. Baerg
National Weather Service, Topeka, Kansas

Ariel E. Cohen
National Weather Service, Topeka, Kansas

1. Introduction and Motivation

The purpose of this research is to identify mesoscale patterns preceding EF3-EF5 tornadoes across eastern Kansas and vicinity, in order to provide meteorologists with scientifically founded clues to anticipate this high-impact weather with lead time. This study involves manual analyses of numerous surface weather charts for the few hours preceding over a dozen EF3-EF5 tornado events. Analyses were subsequently composited using summary statistics to create archetype mesoscale patterns associated with these particularly dangerous phenomena. These results will have the potential to enhance the spatiotemporal precision and accuracy of the National Weather Service's impact-based decision support services (IDSS) by providing meteorologists with tools to

perform mesoanalysis-based pattern recognition corresponding to eastern Kansas and vicinity EF3-EF5 tornado threat areas relative to key boundaries, specifically in the four hours leading up to tornado development.

2. Prior research regarding relative locations of significant tornadoes

Prior research has demonstrated the importance of surface boundaries in enhancing the potential for tornadoes accompanying convection (e.g., Maddox et al. 1980; Davies 1993; Rasmussen et al. 1995; and Markowski et al. 1998). These boundaries are often marked by gradients in integrated and composite parameters, including mixed-layer convective available potential energy (MLCAPE) and significant tornado parameter (STP; Thompson et al. 2012). They can be the focus of overlapping surface-based buoyancy and ample low-level streamwise vorticity. Furthermore, Cohen (2010) identified STP gradient zones as being key foci for violent tornado occurrence, which tend to occur in association with relatively strong 0-1-km storm-relative helicity (SRH).

Markowski (2002) provided comprehensive analyses of the supercell-tornado process. Supercell processes are more likely to favor tornadogenesis when ample streamwise vorticity – vertically integrated to yield SRH – is ingested into the updraft to foster immediate updraft rotation. In turn, this strengthens the supercell's low-level mesocyclone and corresponding perturbation-pressure deficit. This perturbation-pressure deficit promotes storm-underlying vertical stretching and amplification of surface-layer vorticity, which is baroclinically generated in the horizontal and then subsequently tilted and stretched in the vertical. Moreover, boundary-attendant vorticity can be ingested and

strengthened into the storm's updraft (via tilting, stretching, and vertical advection), subsequently further intensifying the surface vorticity in support of tornadogenesis.

The baroclinic generation of horizontal vorticity can arise from storm-induced gust fronts, such as the leading edge of a rear-flank downdraft, and also from the ambient pressure and density contrasts across an antecedent boundary. The latter scenario represents a pre-storm mesoscale factor, and is most typically linked to a tornado-favoring zone of overlapping enhanced SRH and surface-based buoyancy when the boundary behaves as a stationary or poleward-advancing front branching east of a triple point or surface low. Garner (2012) addresses many of the important relationships between tornado development and surface boundaries.

It is clear that precise mesoanalyses of key boundaries within and peripheral to warm sectors theoretically extend to the identification of zones of ambient vorticity ingestion into supercell storms to favor tornadogenesis. This serves as the motivation of the present work – i.e., quantifying the positions of the most significant tornadoes (i.e., those rated EF3-EF5) relative to these potentially favorable zones. Ultimately, such quantification will have the potential to assist forecasters with identifying EF3-EF5 tornado threat areas with increasing precision, lead time, and accuracy following detailed mesoscale analysis.

3. Data and methods

The authors manually analyzed surface maps corresponding to a total of 14 EF3-EF5 tornadoes across portions of eastern Kansas and vicinity for cases as recent as 2016 and extending as far back in time as 1984. The selection of these tornadoes was entirely

arbitrary, though this study is intended to account for a substantial proportion of days during which violent tornadoes occurred across eastern Kansas from 1984 to 2016. Most of the tornadoes in this dataset were rated EF4 (10 cases in this dataset). EF5 tornadoes (two cases in this dataset) are the most exceedingly rare, limiting their sample size, while a couple of particularly impactful EF3 tornadoes that affected the National Weather Service Topeka County Warning Area were included owing to their particularly high visibility and local-area research interests. One of these EF3 tornadoes includes the Bennington, Kansas EF3 tornado of May 28, 2013, which was associated with mobile-radar-sampled wind speeds aloft consistent with those linked to EF4 tornado ratings. The total sample size of tornado days investigated in the present study is ultimately small owing to the rarity of this phenomenon.

For each of the 14 tornado cases, surface charts were carefully hand analyzed for observed mean sea level pressure, temperature, and dewpoint for the observations corresponding to the hour in which the tornado occurred (tornado hour) and each of the four hours preceding tornadogenesis. Hereafter, the term "tornado hour" will be used to generalize the time of tornadogenesis, despite the variability of tornado occurrence time within that hour. This generalization accounts for uncertainty in identifying exactly when a tornado will form, along with the timing of availability of a complete set of conventional surface observations closest to and preceding tornado occurrence. All tornado-preceding times are considered in terms of hours prior to the tornado hour. The analyses of these fields permit the identification of multiple boundaries within and surrounding the warm sectors corresponding to each of the EF3-EF5 tornadoes, and three particular surface features commonly appeared in all cases, as will be subsequently addressed. The

subjectivity of manual analysis is an inherent source of error and lack of reproducibility for this study, as human-crafted analyses vary considerably from analyst to analyst (Sanders and Doswell 1995). Compositing over a dozen cases is expected to remove some of the uncertainty and/or error associated with any given analysis, such that the composite could represent a consensus analysis.

An example of the process for documenting boundaries and a tornado location for each of the four hours preceding and including the hour of the tornado for a specific event (February 28, 2007) is illustrated in Figs. 1 and 2. Figure 1 illustrates a manually analyzed surface chart four hours preceding the tornado hour, following conventional analysis procedures. A few of the features illustrated in Fig. 1 are apparent among all of the tornado cases, and are leveraged as common reference features among all tornado events and times. These include an "intersection point" which marks the intersection of a more meridionally oriented surface dryline or Pacific cold front, and a more zonally oriented baroclinic zone. The cool side of the baroclinic zone is typically marked by antecedent continental air and/or convectively processed air, potentially undergoing moistening/modification owing to poleward mass fluxes. The southernmost extent of the baroclinic zone is hereafter referred to as the "effective boundary," and is indicated by the dashed warm front identified on Fig. 1. The easternmost of the meridionally oriented surface boundaries – i.e., dryline or Pacific cold front – is treated as the western bound of the buoyant sector (dryline for the case of Fig. 1).

In order to create mesoanalysis composites among all four hours for each of the 14 cases, spatial properties of each of the three key surface features and tornado locations were documented. Owing to the aforementioned key relationships between tornado

occurrences and antecedent boundaries, locations of tornadoes are considered in the context of the aforementioned three surface features for each and every analysis time. As such, summary statistics aggregating the boundary spatial properties and relative tornado locations are subsequently determined to generate composite archetype analyses. To highlight this process in an example, Fig. 2 depicts the surface features determined from Fig. 1 re-plotted on a blank map of Kansas and vicinity. To accomplish the consistent documentation of boundary characteristics and boundary-relative tornado locations, the center of a polar coordinate grid was overlaid on the intersection point of each map, as illustrated in Fig. 2. The angular and radial properties of intersection-point-relative boundaries and tornado locations lent themselves to documentation in polar coordinates. This process establishes an intersection-point-relative coordinate system used as the basis for measuring boundary configurations – which a meteorologist can identify in real-time – that can be compared to tornado locations, as illustrated in Fig. 2. The 0° azimuth of the polar coordinate system was aligned parallel to lines of constant latitude.

Following the coordinate system assignment, range and azimuth measurements were documented from each of the analyzed maps. Next, the azimuth of the effective boundary, dryline or Pacific cold front (dryline for the case shown in Fig. 2), and tornado location were determined in a counterclockwise sense from the zero-degree azimuth (Fig. 2). Boundary orientations used to determine these azimuths were constructed by connecting segments between the intersection point and a point along the boundary extending outwards to the range of the tornado. This effectively treats boundaries as linear segments to the tornado range, thus excluding the incorporation of waves and oscillations in the boundary structures. This tornado range was also documented.

In summary, the following data components were collected for each of the four hours preceding tornadogenesis and the hour of tornadogenesis (Fig. 2): (1) range of tornado from intersection point; (2) azimuth of effective boundary (measured counterclockwise from the zonal/west-east-oriented axis [0°] to boundary segment that connects the intersection point and the boundary point at tornado range; and (3) azimuth of easternmost of Pacific cold front or dryline (measured counterclockwise from zonal axis [0°] to boundary segment that connects intersection point and boundary point at tornado range).

The entire scope of data includes each of the previously mentioned three features for the tornado hour and four tornado-preceding hours for all 14 cases. To facilitate consistent compositing, each of the aforementioned data elements – initially based on ranges and azimuths on a polar coordinate system – were projected onto a Cartesian coordinate system with the origin corresponding to the intersection point. Specifically, trigonometric sinusoidal functions were used to project polar coordinates to Cartesian coordinates. This ensures that the relative rank of each data element is unique and based solely on the physical distances from the intersection point, which would be a challenge using a polar coordinate grid system owing to its circular character.

Each of the three data components, projected onto the Cartesian coordinate system, were aggregated within hourly bins for each of the four hours preceding the EF3-EF5 tornado development and the tornado hour. Thereafter, the 25th, 50th, and 75th percentiles of each zonal and meridional component of each of the aforementioned three data components were determined to produce representative spectra of boundary orientations and tornado positions. These summary statistics were used to illustrate the

typical locations and spread of boundaries *relative to the intersection point* and tornado locations for each hour leading up to, and including, the tornado hour. By plotting these statistical positions on a Cartesian coordinate system scaled to a Kansas-centered map, corresponding mesoscale-analysis archetype surface charts were subsequently constructed.

The meteorologist can reference these charts in order to enhance the spatiotemporal precision and accuracy of high-end tornado-threat messaging at lead times spanning upwards of a few hours preceding tornado development. It is critical to note that this study does not distinguish between scenarios favoring EF3-EF5 tornado production and null cases, and a pattern-recognition-based comparison to archetype surface patterns inherently discounts event uncertainty. This is why it is crucial to first identify whether or not the favorable set of necessary conditions for the development of deep moist convection capable of producing such intense tornadoes must become established – e.g., leveraging an ingredients-based assessment and numerous observational and model platforms including convection-allowing model guidance and the Statistical Severe Convective Risk Assessment Model (SSCRAM) (Hart and Cohen 2016) – before tactically messaging refined threat areas and timing.

4. Analysis and Discussion

Figures 3-7 illustrate the archetype composite surface patterns associated with the eastern Kansas and vicinity EF3-EF5 tornado occurrences addressed in the current study, progressing chronologically – hour by hour – in the four hours leading up to tornadogenesis, as well as the tornado hour. These plots are initially provided without reference to specific spatial designations for the purpose of generalization.

Four hours prior to the development of the tornado (Fig. 3), the forthcoming tornado locations are closely aligned with the effective boundary positions. Specifically, the interquartile range of tornado reports spatially overlaps with the interquartile range of boundaries preceding the tornadoes by four hours. In fact, the 50th and 75th percentile tornado report locations, and to some extent the 25th percentile tornado report locations, nearly identically align with the respective boundary-percentile segments. This does not imply that, for *individual* cases, the four-hour-tornado-preceding boundary position was necessarily exactly aligned with the forthcoming tornado location. Rather, in an aggregate sense, there exists mesoscale spatial similarity between effective boundary positions four hours before tornado occurrence and eventual tornado occurrence. Also of note, Fig. 3 illustrates that the interquartile range of tornado positions is removed well to the east of the intersection-point location four hours before the EF3-EF5 tornado hour. In fact, both the 50th and 75th percentiles are displaced to the east of the intersection point by over 100 miles. With the intersection point representing a focused area of relatively stronger forcing for ascent, these finding suggests that these intense tornadoes were occurring in relatively weaker forcing-for-ascent regimes and are critically reliant on the effective boundary presence.

Three hours prior to the tornado (Fig. 4), an overall alignment of tornado locations with tornado-preceding boundary positions is apparent. However, there appears to be a slight southward spread of the interquartile range of tornado positions within the warm sector from four hours to three hours preceding tornadogenesis (comparing Figs. 3 and 4). This is especially the case for the 25th and 50th percentile tornado positions. Also of note, the interquartile range of tornado reports is found to narrow to some extent from four

hours to three hours preceding tornadogenesis, with the 50th and 75th percentile tornado reports shifting westward and closer to the intersection point by about 20-40 miles and the 25th percentile of tornado reports shifting eastward away from the intersection point. Nevertheless, these tornadoes are still found to occur well east of the intersection-point location. The plot depicting statistical tornado and boundary positions preceding EF3-EF5 tornadoes by three hours (Fig. 4) is quite similar to two hours preceding the tornado hour (Fig. 5).

One hour prior to the tornado (Fig. 6), the southernmost part of the interquartile range of tornado points is found to continue a southward spread – i.e., deeper into the warm sector – (compared to Fig. 5 for 2 hours preceding tornadogenesis), while the 50th and 75th tornado-location percentiles are found to remain closely aligned to the tightly clustered interquartile range of effective boundary locations. There appears to be noticeable spatial spread between the 25th percentile of the effective boundary and 25th percentile of the tornado locations. This highlights two general spatial regimes at one hour preceding EF3-EF5 tornado occurrence: tornado reports in the open warm sector that were previously lying in proximity to the effective boundary one hour before tornadogenesis, and a cluster of reports aligning with the one-hour-before-tornado effective boundary positions. The overall pattern during the tornado hour (Fig. 7) is similar to the prior hour (Fig. 6).

Comparing Figs 3-7, there are also oscillations in the zonal width of the interquartile range of tornado locations. This includes the narrowing of this width from four hours to three hours before tornadogenesis (comparing Figs. 3 and 4) as previously discussed, a more subtle narrowing of this width from two hours preceding tornadogenesis

(Fig. 5) to one hour prior to tornadogenesis (Fig. 6), and a westward shift in the entire interquartile range of tornado locations from one hour prior to tornadogenesis to the tornado hour (comparing Figs. 6 and 7). Some of these oscillations may be explained by the motion of the surface features during the hours leading up to tornadogenesis, and potential uncertainty inherent to their analyzed positions. Additional work would be required address physical explanations for these zonal shifts, however a notable finding is that these corridors are all displaced well to the east of the intersection point. Moreover, these statistical analyses quantify approximate spatial bounds for tornadoes locations relative to boundaries and intersection points that can be revealed by real-time mesoanalysis, based on observed meteorological data and storm reports.

Overall, Figs. 3-7 offer meteorologists with pattern-recognition-based means for generating quantifiable and reproducible estimates of EF3-EF5 tornado potential across eastern Kansas and vicinity based upon composited mesoscale analysis. By identifying a favorable thermodynamic and kinematic parameter space for these intense tornadoes, it may be possible to tactically refine messaging, focusing on the intersection-point-relative threat areas identified in these figures. A mesoscale analyst will have the capability of identifying threat areas based on these charts after having performed accurate mesoscale analysis, identifying a favorable environment for these intense tornadoes, and determining time of most likely tornado occurrence.

5. Operational Applications

Pairing the aforementioned precursor clues to observed boundaries permits messaging of corresponding threat areas based on Figs. 3-7. This is demonstrated directly as a proof-of-concept example for a tornado that developed west of Bennington, Kansas on May 25, 2016 and tracked toward areas near Chapman, Kansas where it produced EF4-rated damage – within the National Weather Service Topeka, Kansas County Warning Area.

Figures 8-12 plot the chronological progression of intersection point locations and attendant analyzed boundaries leading up to the tornado hour. These figures depict overlays of the corresponding statistical boundary positions and tornado threat areas, via interquartile ranges, relative to the analyzed intersection point locations – effectively transposing the summary statistics from Figs. 3-7 onto Figs. 8-12. The 25th, 50th, and 75th percentile boundary positions are plotted in Figs. 8-12 to represent the statistical boundary positions, while a multi-shade, color-filled rectangle is shown on each figure, which connects the bounds of the interquartile range representing the tornado threat area. If a meteorologist were to determine a certain environment as being favorable for EF3-EF5 tornado development, he or she could identify the upcoming tornado threat area based on the identified intersection point and expected time of tornadogenesis, as demonstrated in Figs. 8-12, and then compare analyzed boundaries to the corresponding statistical boundary distributions to refine the most likely EF3-EF5 tornado threat area. These figures also permit comparison between the estimated tornado threat area in the few hours leading up to tornadogenesis and the actual location of the tornado.

Four hours prior to tornado development, Fig. 8 highlights the intersection point near Great Bend, Kansas, south of which a wavy outflow boundary extends east-northeast

toward Manhattan, Kansas with a dryline (including an embedded dryline surge south of the intersection point) extending into northwestern sections of Oklahoma. The tornado occurred within the northern part of the implied threat area, based on the four-hour-preceding-tornado mesoscale analysis.

Three hours before the tornado developed west of Bennington, Kansas (Fig. 9), the actual tornado occurrence coincided with the edge of the corresponding threat-area rectangle, which has shifted a bit farther south of the tornado location. This highlights how the illustrated threat area should not be considered as being accompanied by rigid edges in practice, but rather be considered as accompanied by smoothed threat gradations around the edges. This is especially the case, since the interquartile ranges may be influenced by analysis uncertainty. It is particularly noteworthy that the tornado location is found to lie along the effective boundary position preceding the tornado by three hours, with the position of this boundary appearing as quasi-stationary (comparing Fig. 9 to 10 to 11 to 12). If a forecaster were to anticipate this boundary being accompanied by negligible motion in the hours leading up to tornadogenesis, then that could encourage the forecaster to ensure that the messaged threat area extends to the observed boundary position owing to the significance of boundary interactions favoring tornadogenesis, potentially warranting an extension of the statistically defined threat area.

Figures 10-12 show the proximity of eventual tornado occurrence to the mesoanalysis-based threat areas preceding tornadogenesis by 1-2 hours and during tornado hour. The temporary zonal narrowing of the threat area for one hour preceding tornado development prevents the tornado from being encompassed in the threat area, though the tornado was still in proximity to this threat area and along the quasi-stationary

boundary. Implying a loose, non-rigid bound to the exact threat area would be key in accurately messaging the most-likely tornado threat area to encompass a sufficiently large threat area hours in advance – especially given a foundational sample size that is as small as it is in the present study. It is clear that this tornado was one clustered in the regime of near-effective boundary cases as opposed to open-warm-sector cases.

This individual case demonstrates how effective mesoanalysis can be leveraged for identifying tactical threat areas by a few hours prior to the development of a particularly intense tornado. The present study offers the scientific foundation for translating the manual mesoanalysis to tactical messaging. Figures 12-13 demonstrate the direct research-to-operations approach to this type of analysis. For instance, a mesoscale analyst may analyze a 2000 UTC surface chart – as shown in Fig. 13. After identifying the most probable time frame for intense tornado occurrence being in a few hours, the meteorologist could then assign a tornado threat area based on Fig. 8 corresponding to intersection-point-relative tornado threat areas preceding tornadogenesis by four hours. Figure 14 displays the four-hour-preceding-tornado threat area on an example enhanced short-term weather outlook graphic. Such a graphic could be displayed on the local National Weather Service website, sent through social media sites, and e-mailed directly to emergency managers and other National Weather Service partners to enhance impact-based decision support services (IDSS). This tactical threat area entirely leverages the research results documented throughout this study, and demonstrates the service end of providing more meaningful, user-relevant information to aid in proactive efforts to prepare for hazardous weather.

6. Summary

This study provides the basis and tools for identifying the area of greatest threat for experiencing EF3-EF5 tornadoes across eastern Kansas and vicinity, with enhanced precision based on mesoscale analysis. The tactically delineated threat areas that follow mesoscale analysis for upwards of four hours preceding the hour of EF3-EF5 tornado development permit messaging of threats at a spatial scale smaller than convective watches, though larger than convective warnings, offering the potential to more accurately depict the spatial focus of highly impactful weather. This can ultimately improve impact-based decision support services.

A total of 14 EF3-EF5 tornadoes that affected eastern Kansas and vicinity were identified. Surface observations were manually analyzed for effective boundaries, Pacific cold fronts, and drylines, along with boundary intersection points, for each of the four hours preceding tornado development along with the hour of tornado occurrence. These surface features were compared to the tornado location for each of these analysis. Compositing of the coordinates of these features projected onto a Cartesian grid system permits the identification of interquartile ranges of boundary positions, tornado locations, and tornado threat areas based on the intersection points.

In addition to the identification of threat areas that can be identified for a few hours preceding EF3-EF5 tornado development, which can extend to science-based service improvements, the present study also reveals multiple physical relationships between tornado threat areas and analyzed surface features. Three to four hours before EF3-EF5 tornado initiation, the eventual tornado location is typically aligned with the effective boundary position. Progressing forward in time, broader EF3-EF5 tornado threat areas

elongate southward, such that during the tornado hour and during the previous hour, tornado positions were largely grouped into two regimes: open warm sector and near effective boundary. These results collectively highlight the sensitivity of intense tornado production to warm sector shapes and peripheral boundary characteristics. The proximity of many of these tornadoes to surface boundaries is physically consistent with the role of these boundaries and environments of their surroundings to locally enhance tornado potential.

Another result of this research is that EF3-EF5 tornadoes are more likely to occur over 50 miles east-southeast, east and northeast of the intersection point, which suggests that these tornadoes are occurring in a regime well removed from stronger forcing for ascent in proximity to the intersection point. As such, their reliance on mesoscale mass fields warrants paramount attention for mesoscale analysis to ensure that their corresponding severe-weather threat area can be accurately depicted. Their parent thunderstorms may have developed along the dryline or in closer proximity to the intersection point, though their eventual interaction with the zone surrounding the downshear effective boundary could be critical for locally enhancing the tornado risk.

This study has provided tangible, applicable means for identifying threat areas of EF3-EF5 tornadoes based on mesoscale analyses of surface observations. Upon establishing the presence of a favorable environment for such high-impact weather, the application of this research is demonstrated to tactically identify a threat area well in advance (upwards of four hours) of a violent tornado that affected a portion of north-central Kansas. This is one example of how composited mesoscale analysis provides an

opportunity to serve as the foundation for improving the spatiotemporal precision and accuracy of severe-thunderstorm threat messaging.

The work demonstrated in the present study will have the potential to be expanded to other convective hazards. More importantly, much larger sample sizes will need to be assessed in order to provide more robust results. The sample size in the present study is relatively small, which warrants implied generalization when interpreting the bounds of implied threat areas. However, larger sample sizes serving as the foundation of subsequent analyses could yield a broader distribution of possible threat area bounds and boundary positions – representative of a more complete spectrum of EF3-EF5 tornado scenarios. Other spatially focused regimes across the country could be the subject of mesoscale-analysis compositing procedures similar to what was done in the present study, whereby the smaller-scale compositing analyses could reveal mesoscale mass-field perturbations that may otherwise be unresolved by compositing across a broader scale.

Ultimately, the present study provides the science-based foundation for messaging intense tornado threat areas with lead times upwards of four hours. This work provides the tools and resources for the mesoscale analyst to apply composite analyses as the scientific foundation for cultivating tactical threat assessments. A direct result of this work is to enhance the accuracy and precision of corresponding messaging. This type of work not only is directly applicable to EF3-EF5 tornado threat assessment across eastern Kansas and vicinity, but is also applicable as a methodology to identify high-impact weather threat areas sensitive to mesoscale mass fields that offer meteorologists clues to identify associated hazards. By leveraging these tools and resources based on mesoscale meteorology, there exists opportunity to make substantial strides in serving the National

Weather Service's partners with more relevant, precise, and accurate information to assist in their decision making to, in turn, build a Weather-Ready Nation.

Acknowledgements

References

Cohen, A. E., 2010: Indices of violent tornado environments. *Electron. J. Oper. Meteor.*, 11, 2010-EJ6. [Available online at http://www.nwas.org/ej/pdf/2010-EJ6.pdf.]

Davies, J. M., 1993: Three strong tornado events in 2008 associated with boundary intersections and narrow instability axes near 700-mb lows. Preprints, *23rd Conf. Severe Local Storms*, St. Louis, MO, Amer. Meteor. Soc., P3.14.

Garner, J. M., 2012: Environments of significant tornadoes occurring within the warm sector versus those occurring along surface baroclinic boundaries. *Electronic J. Severe Storms Meteor.*, **7** (5), 1–28.

Hart, J. A., and A. E. Cohen, 2016a: The Statistical Severe Convective Risk Assessment Model. *Wea. Forecasting*, **31**, 1697–1714.

Maddox, R. A., L. R. Hoxit, and C. F. Chappell, 1980: A study of tornadic thunderstorm interactions with thermal boundaries. *Mon. Wea. Rev.*, **140**, 322–336.

Markowski, P. M., E. N. Rasmussen, and J. M. Straka, 1998: The occurrence of tornadoes in supercells interacting with boundaries during VORTEX-95. *Wea. Forecasting,* **13,** 852–859.

——, 2002: Hook echoes and rear-flank downdrafts: A review. *Mon. Wea. Rev.*, **130**, 852–876.

Rasmussen, E. N., S. Richardson, J. M. Straka, P. M. Markowski, and D. O. Blanchard, 1995, The association of significant tornadoes with a baroclinic boundary on 2 June 1995. *Mon. Wea. Rev.*, **110**, 136–151.

Sanders, F. and C. A. Doswell III, 1995, A case for detailed surface analysis. *Bull. Amer. Meteor. Soc.,* **76**, 505–521.

Thompson, R. L., B. T. Smith, J. S. Grams, A. R. Dean, and C. Broyles, 2012: Convective modes for significant severe thunderstorms in the contiguous United States. Part II: Supercell and QLCS tornado environments. Wea. Forecasting, 27, 1136–1154.
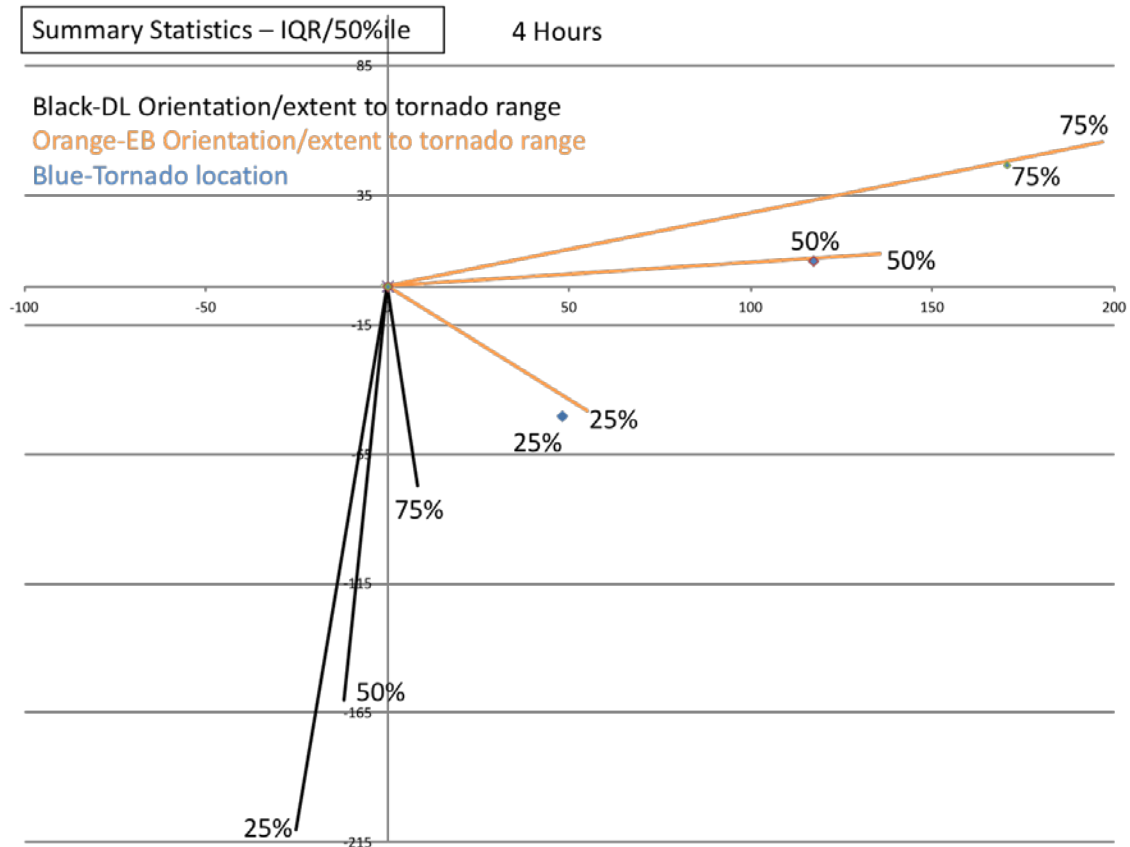
Figures
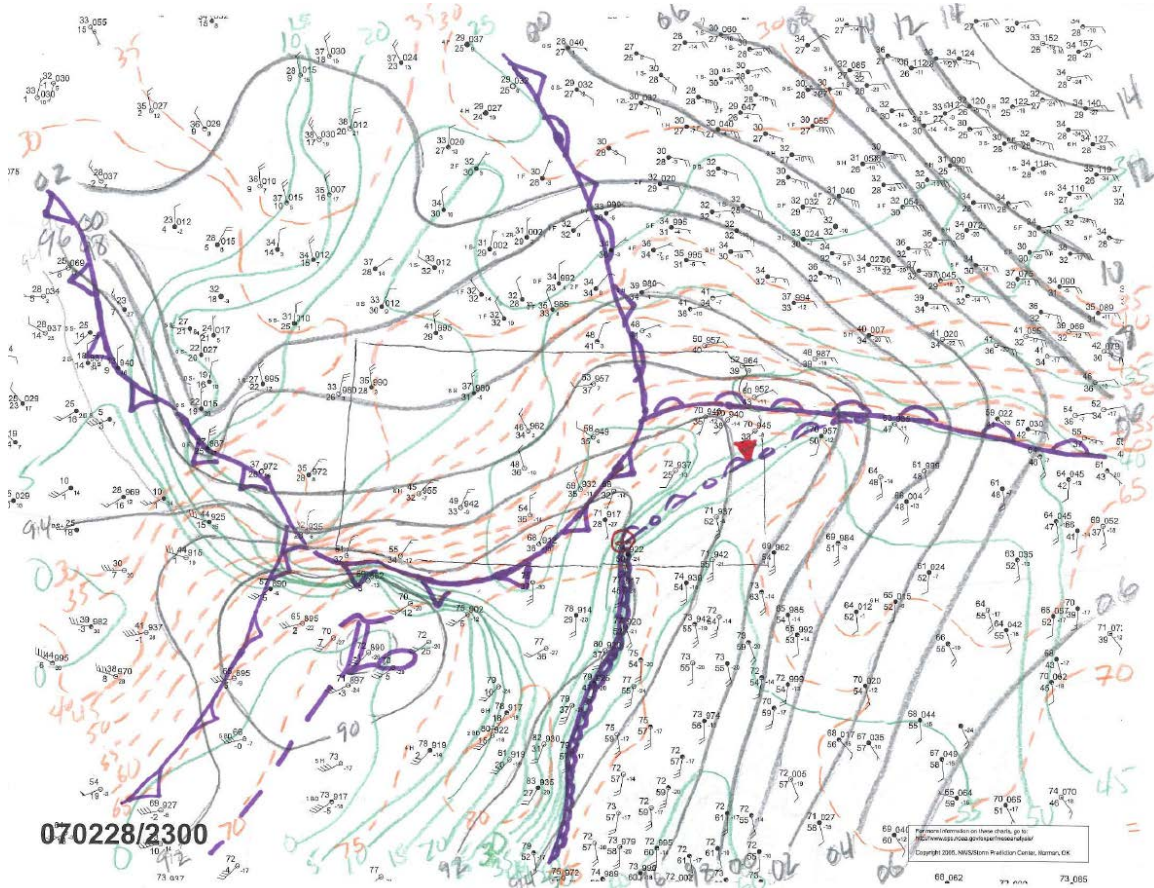
Figure 1. Hand-analyzed surface map from 2300 UTC February 28, 2007, 4 hours before the tornado hour. Dark grey contours represent isobars (mb at 2-mb increments), green contours represent isodrosotherms (°F at 5°F increments), red dashed contours represent isotherms (°F at 5°F increments), red triangle in far eastern Kansas represents violent tornado location, and boundaries and surface low are marked using purple-outlined symbols following standard plotting conventions.
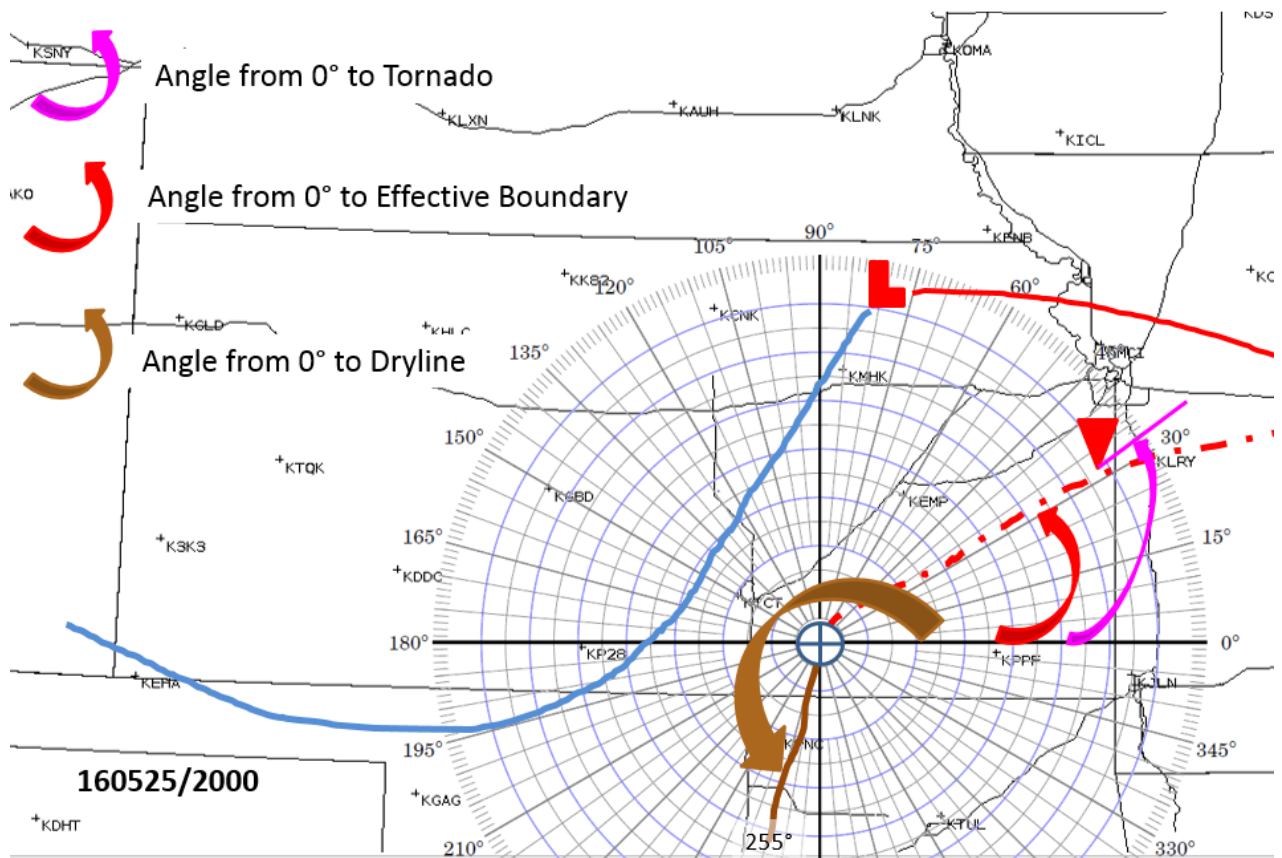
Figure 2. Demonstration of boundary orientation and tornado location identification. This case demonstrates the process of identification for four hours prior to the tornado hour, and corresponds to the surface chart shown in Fig. 1. Surface features from Fig. 1 are overlaid on the map, with the red arc indicating the synoptic warm front, the blue arc indicating the cold front, the red-dashed segment indicating the effective boundary, the brown segment indicating the dryline, and the red "L" symbol indicating the synoptic-scale surface cyclone center. The center of the polar coordinate system has been superimposed on the intersection point. Azimuthal measurements from the 0° axis (i.e., zonal component) of this coordinate system to the tornado, effective boundary, and dryline – in a counterclockwise direction – are reflected by the arching arrows in magenta, red, and brown, respectively. Note that all boundary segments are determined

by connecting the intersection point to a point lying along the analyzed boundary segment at the range of the tornado. For this example, the range and azimuth of the tornado are 115 miles and 32°, respectively, the orientation of the effective boundary is 30°, and the orientation of the dryline is 255°.

Figure 3. Representations of statistical-composite boundary orientations emanating from an intersection point (origin), with effective boundary (EB) orientations depicted by dark orange lines and orientations of the dry line (DL) – also incorporating Pacific cold fronts – depicted by black lines, for four hours preceding the development of the EF3-EF5 tornado. These orientations are computed by determining the 25th, 50th, and 75th percentiles – also known as the interquartile range (IQR) – of the x- and y-components of the respective boundary endpoints for each tornado case at the corresponding tornado range, following projection of these endpoints from the polar coordinate system (yielding azimuths and ranges) to a Cartesian coordinate system (yielding x- and y-coordinates). In a similar manner, the 25th, 50th, and 75th percentile of the x- and y-components of EF3-EF5 tornado locations following projection of the polar coordinates to Cartesian

coordinates, centered on the intersection point, are plotted by the small blue markers.

Boundary and tornado-location percentiles are annotated by percentages. Markers along

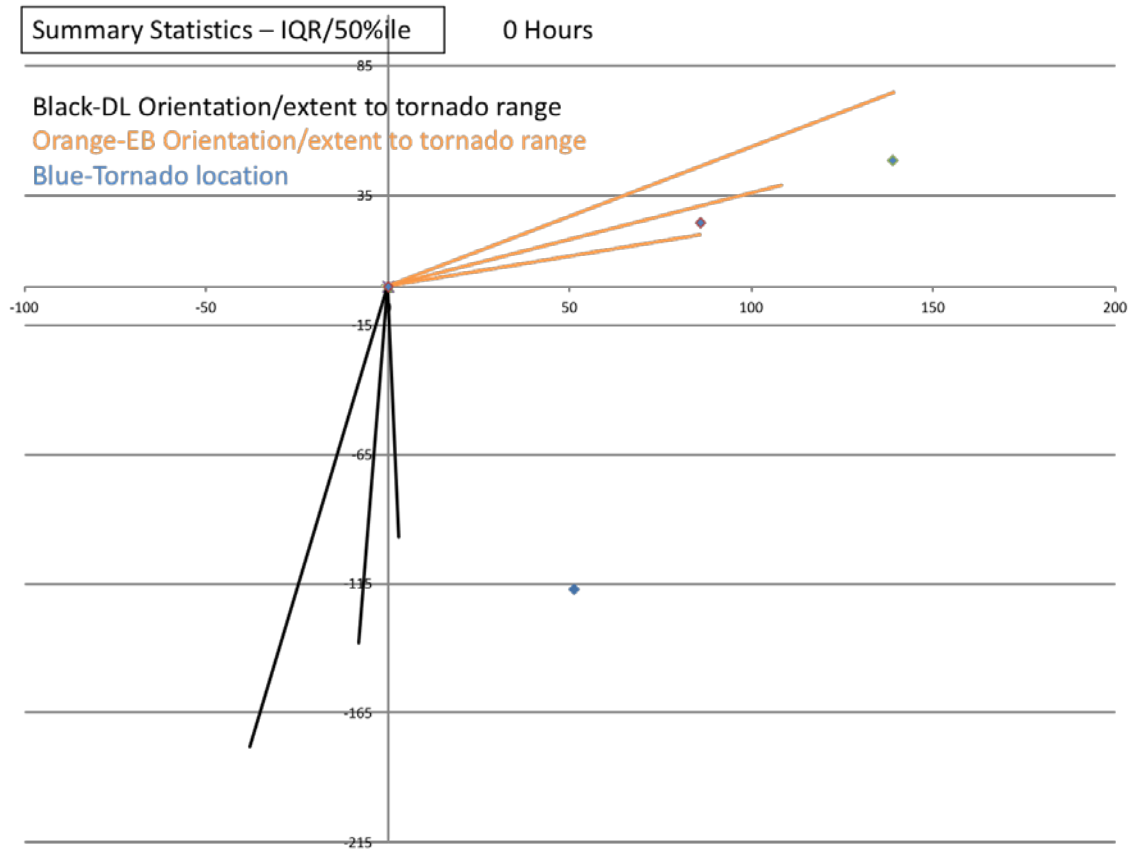the x- and y-axes are referenced with units of miles.
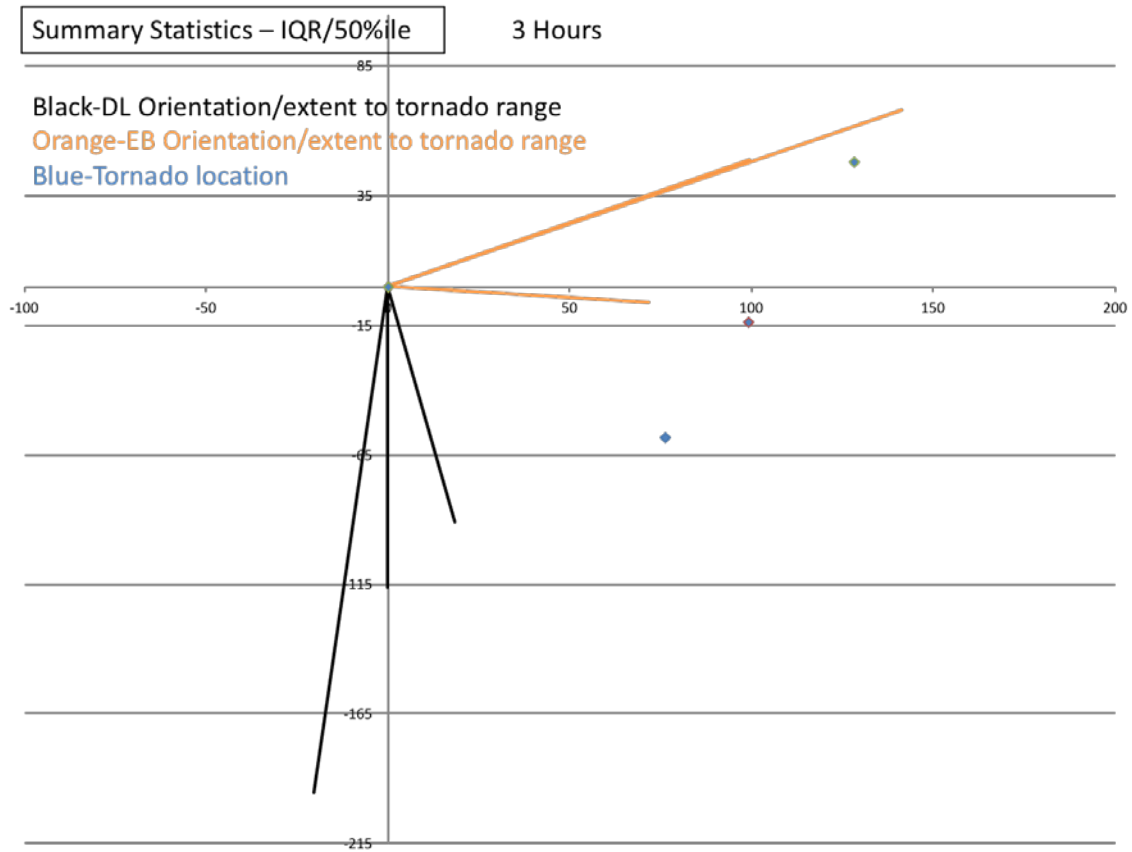
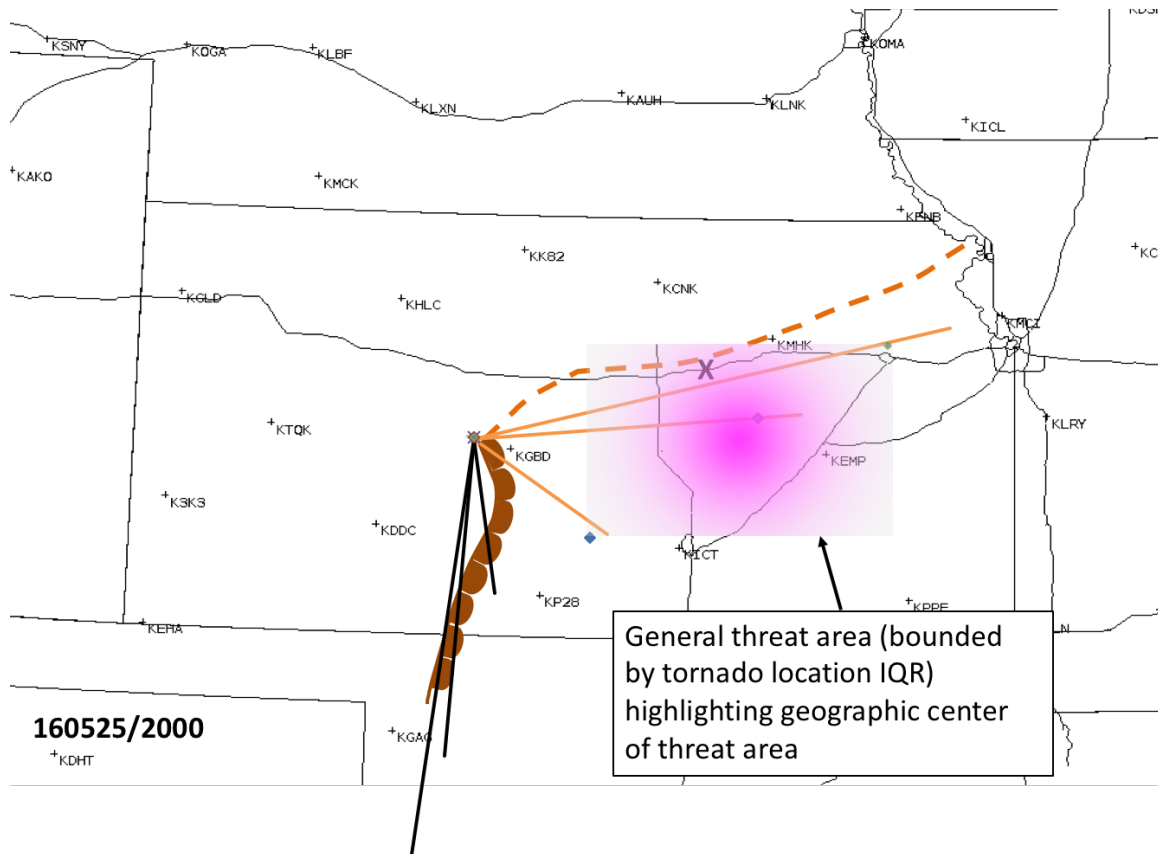**Figure 4.** As in Fig. 3, except three hours prior to tornado hour.
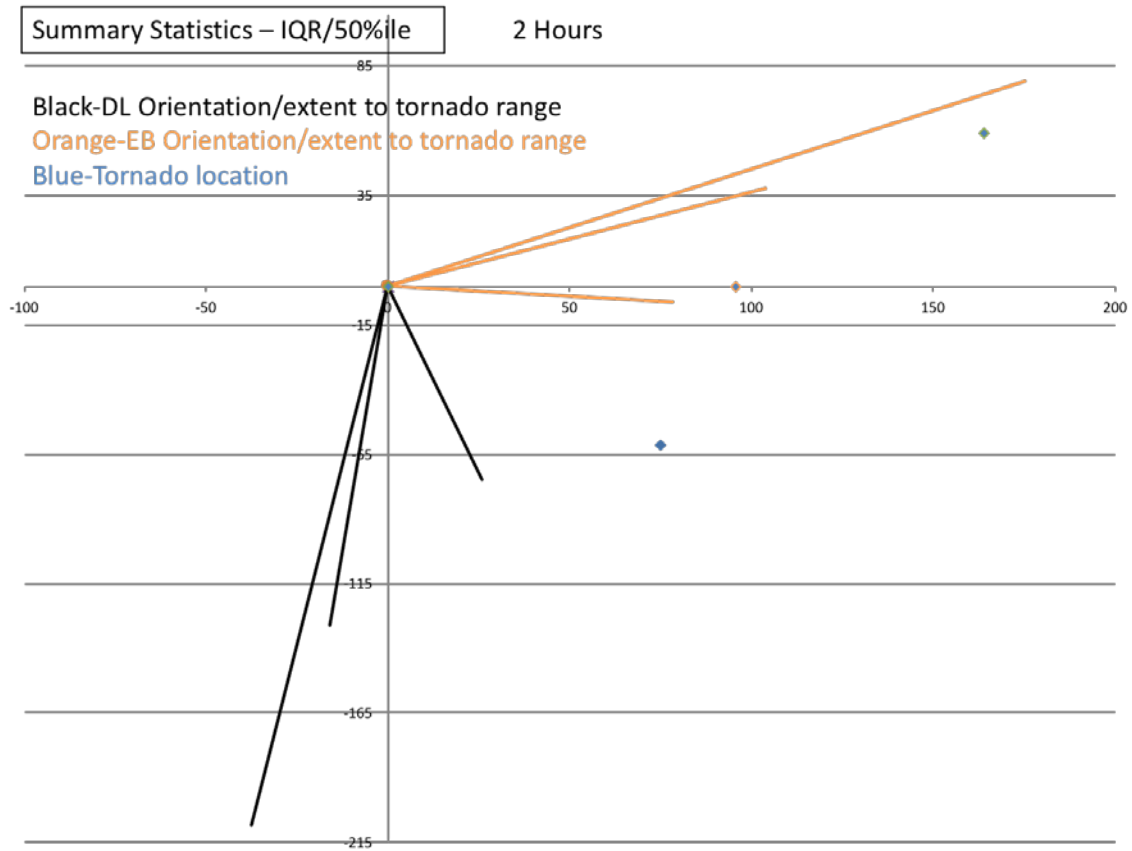
Figure 5. As in Fig. 3, except two hours prior to tornado hour.
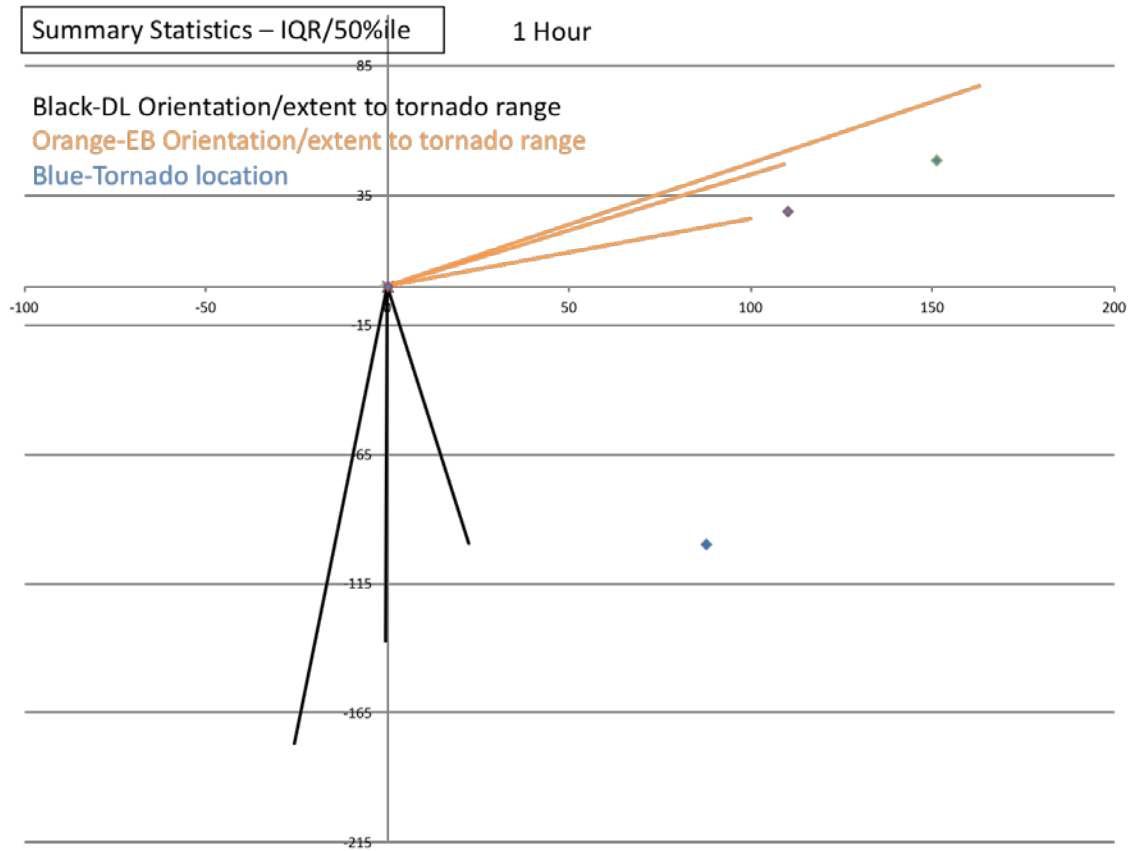
**Figure 6.** As in Fig. 3, except one hour prior to tornado hour.

Figure 7. As in Fig. 3, except for the tornado hour.

Figure 8. Surface boundaries preceding the Bennington-Chapman, Kansas area EF4 tornado by four hours relevant for identifying the tactical threat area for EF3-EF5 tornadoes. The effective boundary is indicated by a dashed brown line extending east-northeast of a triple point analyzed west of Great Bend, Kansas (KGBD) south of which a dryline extends. The composite-statistical boundary positions and composite-statistical tornado locations plotted in Fig. 3 are overlaid by aligning their accompanying intersection point with the observed triple point and scaling the overlay to ensure consistency with the Kansas-centered plotting illustrated in this figure. A multi-shaded, magenta-color-filled rectangle is plotted by connecting the extrema of the tornado-location interquartile ranges to identify a boundary-relative EF3-EF5 tornado threat area for four hours into the future, with the darkest color shading located at the geographic

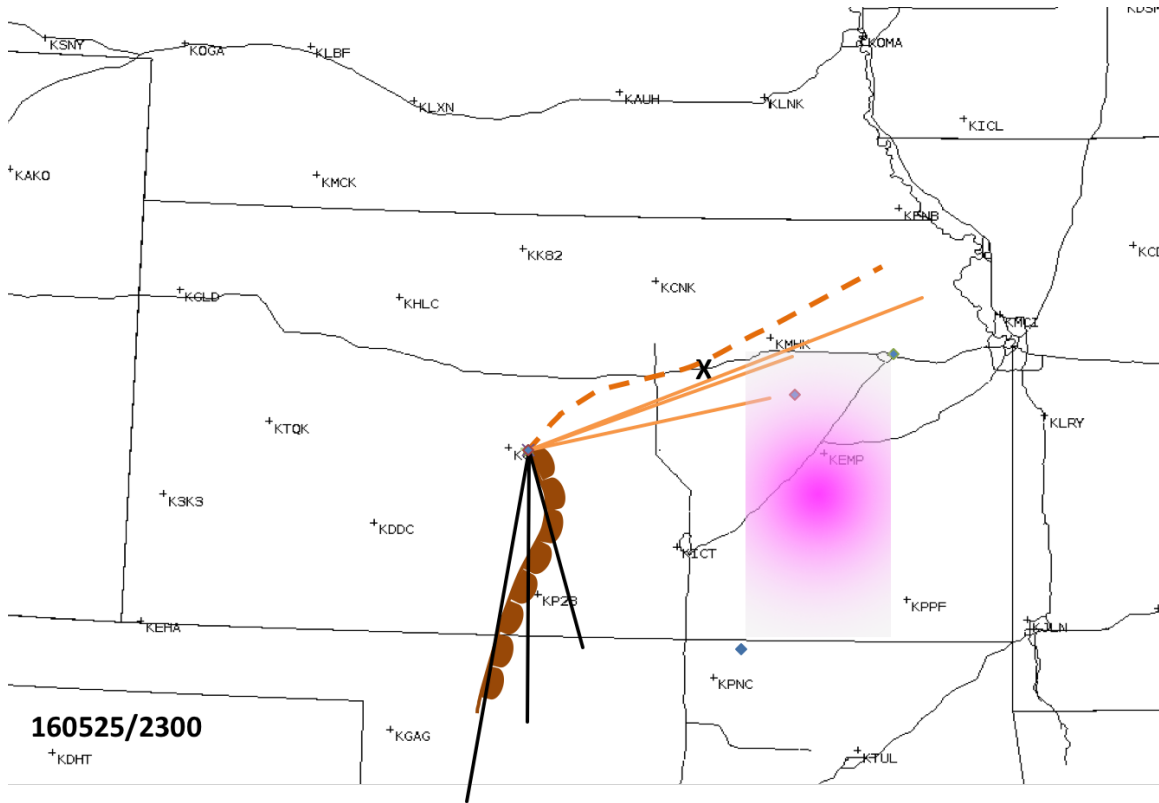center of this rectangle and lighter shading extending radially outward from this center. The location of tornado occurrence is marked by the letter "x".
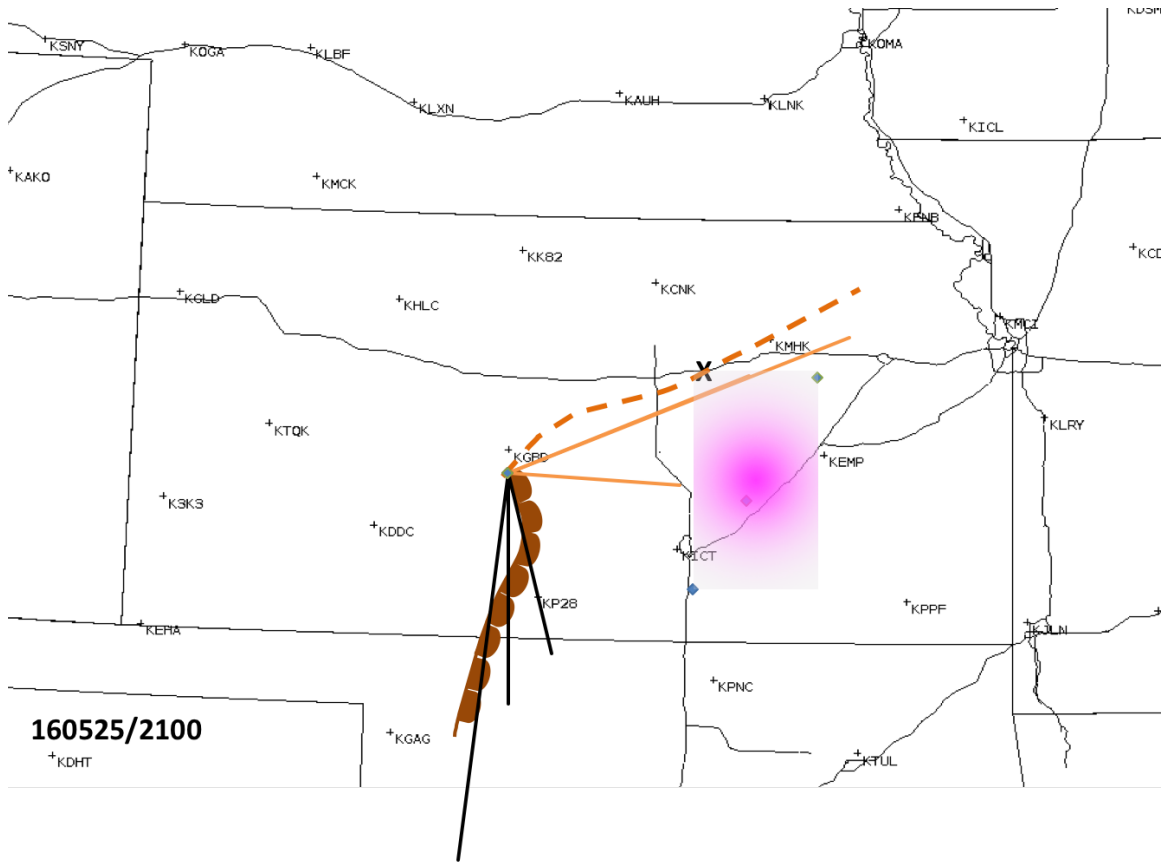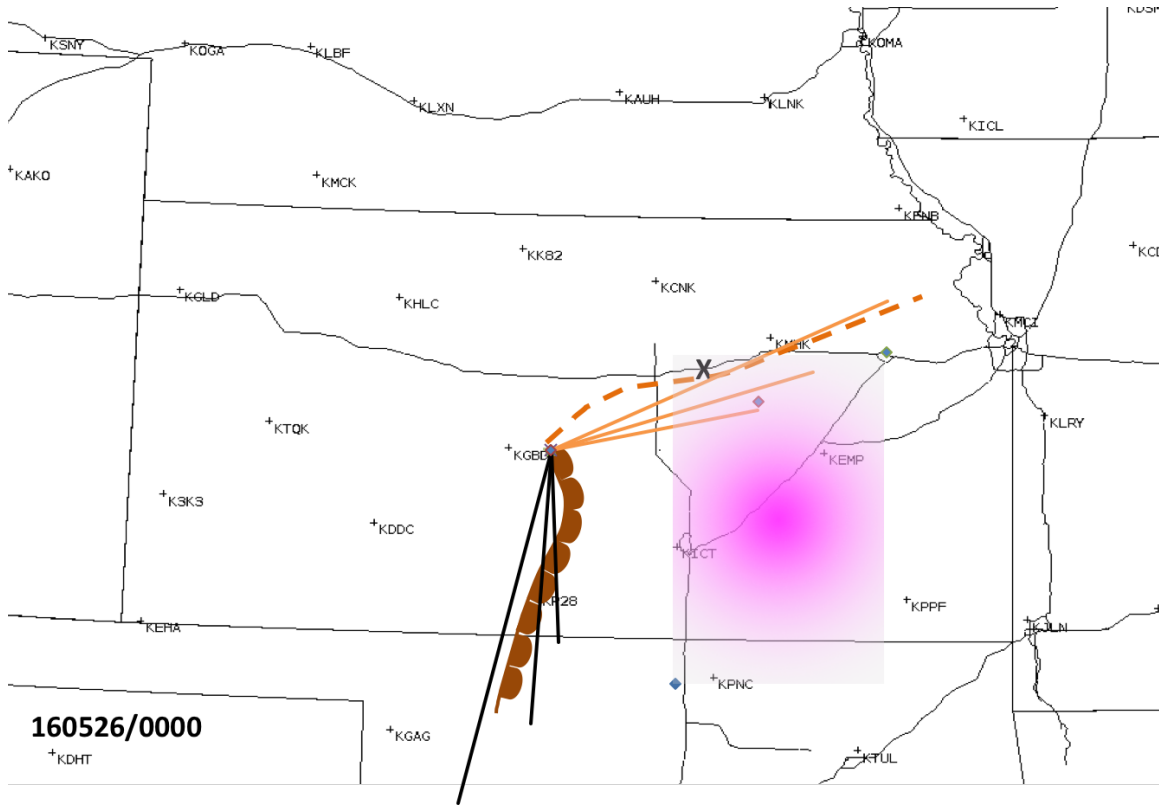

Figure 9. As in Fig. 8, except for three hours preceding the tornado hour.
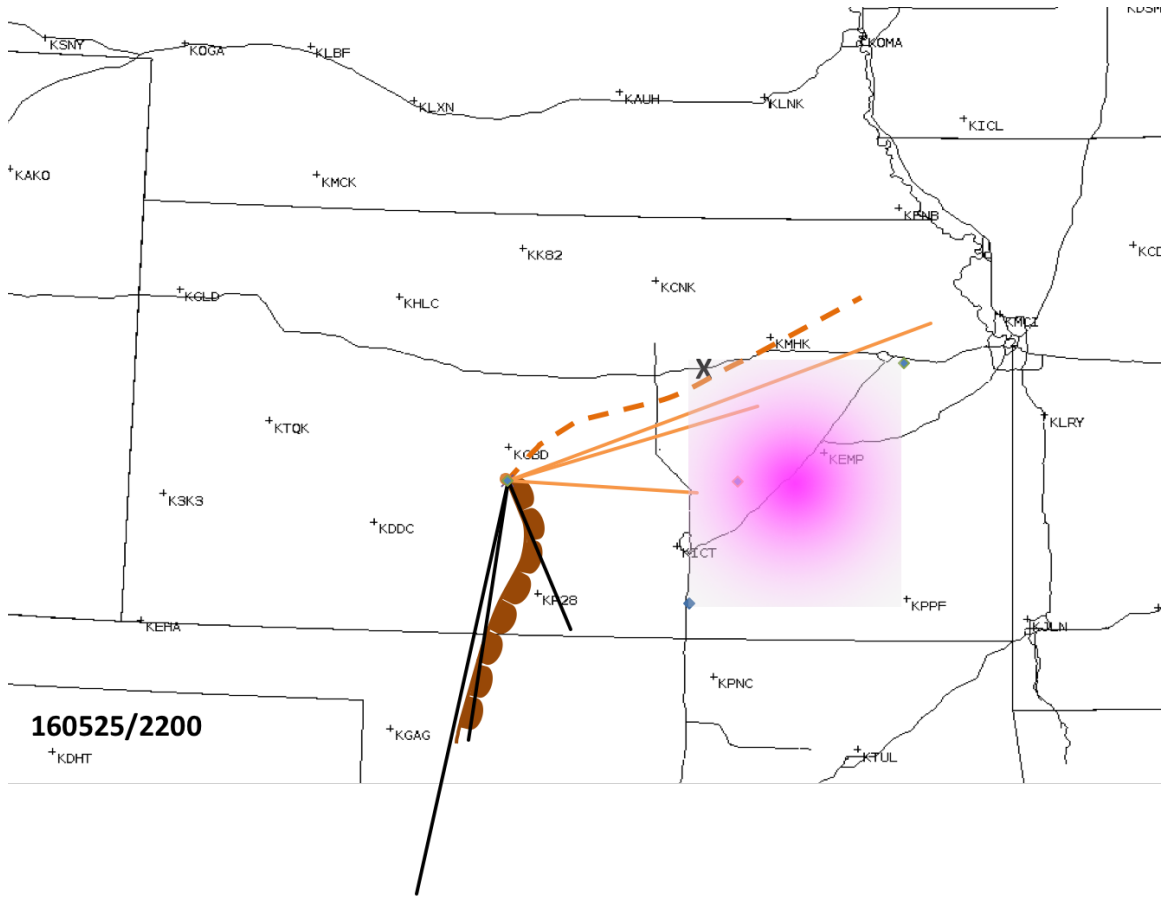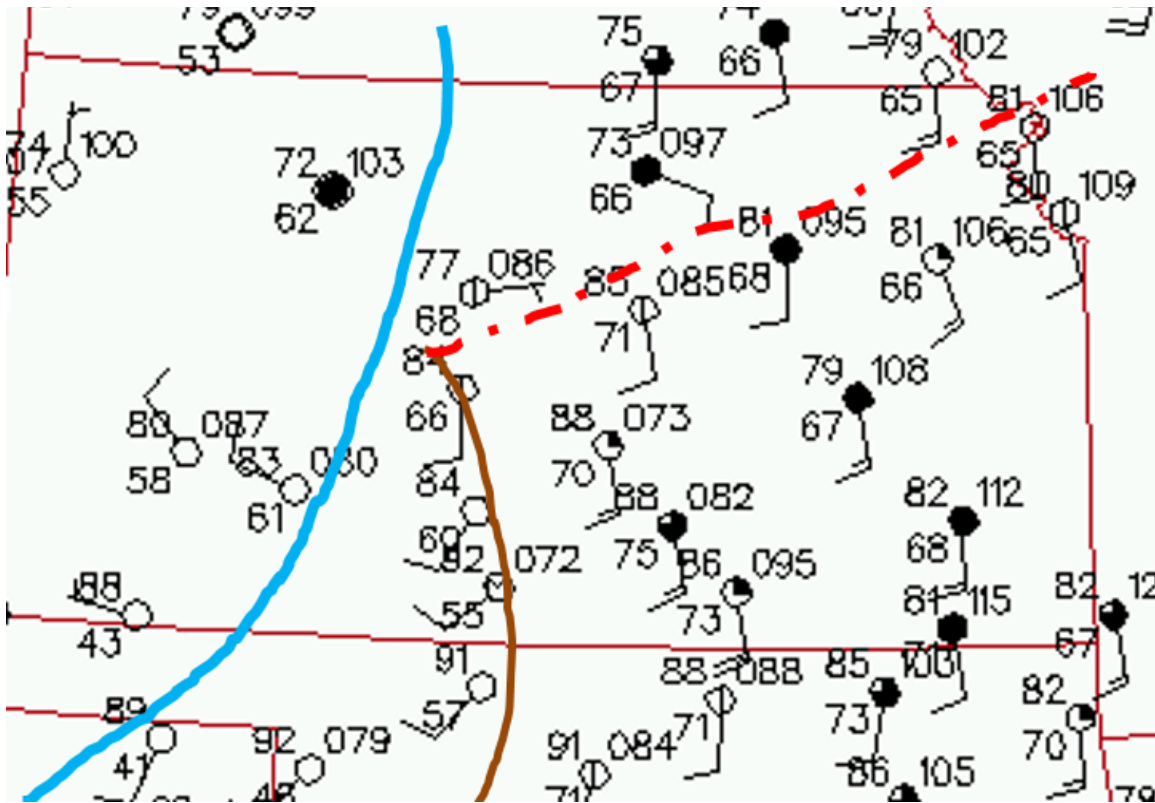
**Figure 10.** As in Fig. 8, except for two hours preceding the tornado hour.

Figure 11. As in Fig. 8, except for one hour preceding the tornado hour.

Figure 12. As in Fig. 8, except for the tornado hour.

Figure 13. Illustration of a hand-analyzed surface chart at 2000 UTC preceding the

Bennington-Chapman, Kansas tornado of May 25, 2016, which can be crafted in real

time by a mesoscale analyst. This corresponds to the boundaries identified in Fig. 8.

Surface observations are plotted with an overlay depicting the effective boundary in the

dashed red contour, and the arching brown contour depicting the dryline. The

intersection of these two boundaries is referred to as the "intersection point" throughout

this study. Finally, the blue arching contour indicates the cold front.
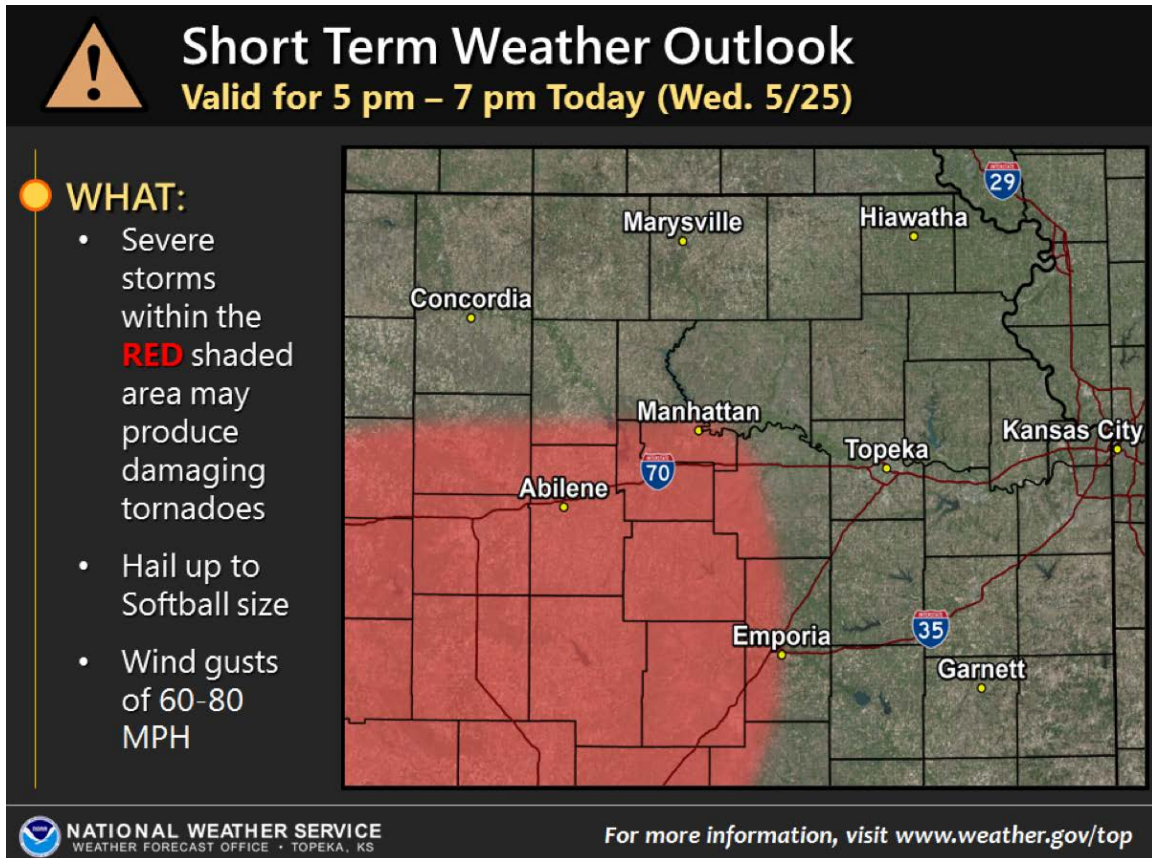
Figure 14. An example of an example enhanced short-term weather outlook enhancing IDSS for NWS partners leading up to the May 25, 2016 Chapman, Kansas tornado. This graphic identifies a tactical threat area based upon the mesoscale analysis shown in Fig. 13 preceding the development of EF3-EF5 tornado potential by four hours. The specific bounds of this area are based upon the EF3-EF5 tornado threat area depicted by the model depicted in Fig. 8.